Metallic Junction Thermoelectric Device Simulations

Adam J. Duzik*[a] and Sang H. Choi[b]
[a]National Institute of Aerospace, 100 Exploration Way, Hampton, VA, 23666
[b]NASA Langley Research Center, 8 West Taylor St., Hampton, VA, 23681

ABSTRACT

Thermoelectric junctions made of semiconductors have existed in radioisotope thermoelectric generators (RTG) for deep space missions, but are currently being adapted for terrestrial energy harvesting. Unfortunately, these devices are inefficient, operating at only 7% efficiency. This low efficiency has driven efforts to make high-figure-of-merit thermoelectric devices, which require a high electrical conductivity but a low thermal conductivity, a combination that is difficult to achieve. Lowered thermal conductivity has increased efficiency, but at the cost of power output.

An alternative setup is to use metallic junctions rather than semiconductors as thermoelectric devices. Metals have orders of magnitude more electrons and electronic conductivities higher than semiconductors, but thermal conductivity is higher as well. To evaluate the viability of metallic junction thermoelectrics, a two dimensional heat transfer MATLAB simulation was constructed to calculate efficiency and power output. High Seebeck coefficient alloys, Chromel (90%Ni-10%Cr) and Constantan (55%Cu-45%Ni), produced efficiencies of around 20-30%. Parameters such as the number of layers of junctions, lateral junction density, and junction sizes for both series- and parallel-connected junctions were explored.

Keywords: Thermoelectrics, Seebeck Effect, Thermal power generation, Simulation, Microfabrication, Nanofabrication

1. INTRODUCTION

Current thermoelectric power conversion methods rely on semiconductor devices. The heat source causes a migration of excess electrons and holes in the n- and p-type semiconductor legs, resulting in a current flow. Efficiency and device quality are often compared with the figure of merit ZT, given in Eq. 1.[1,2]

$$ZT = \frac{S^2 \sigma T}{\kappa} \quad (1)$$

In Eq. 1, ZT is the dimensionless figure of merit, S is the Seebeck coefficient of the two materials at the junction in V/K, σ is the electrical conductivity in $1/\Omega \cdot m$, T is absolute temperature in K, and κ is thermal conductivity in $W/m \cdot K$. Attempts to manipulate the figure of merit often result in synthesizing materials or fabricating complex device structures with a high σ and a low κ, a rather unnatural combination. Despite decades of intense research to increase the ZT figure of merit, thermoelectric device construction has fundamentally not varied from that in Fig. 1a, and thus still suffers from a low conversion efficiency of 7%;[3] for typical radioisotope thermoelectric generators (RTGs), this comes to about 5W of electrical power per kg, or W_e/kg. Moreover, as κ continues to shrink, the figure of merit increases, but at a cost to power density. At a κ of 0, all heat flow would cease. No thermal energy movement is possible, and thus no temperature gradient is possible, and thus no carriers and no power would be generated. At a cost of approximately $10,000/kg payload at the lowest end, such low efficiency and power density are unsuitable for the rapidly expanding space technology sector and further efforts at manned space exploration.[4]

Other technologies have been proposed as alternatives to thermoelectric generators:

- Thermophotovoltaic cells harness the infrared radiation off of heat sources. While they are more efficient, their manufacturing is complicated, involving III-V semiconductors and filters to return photons of sub-optimal wavelength to the source. Hence, they have not supplanted thermoelectric devices.[5–21]

*adam.j.duzik@nasa.gov; phone 1 757 864-6030; www.nasa.gov

- Thermionic emission is a much simpler form of thermal to electricity conversion, requiring only a metallic emitter and a collector separated only by a small gap. The required vacuum, space charging at the emitter tip, and the difficulty in making nanometer-sized gaps limit this technology.[16,22–27]
- The Advanced Stirling Radioisotope Generator (ASRG) was a high efficiency (~30%) system developed for deep space missions. This system contained gases that expand from the heat source, driving the piston to generate power. Development ended in 2013; only a few prototypes remain. Despite the promised high power, a mechanical system may not have the longevity for deep space missions .[28–36]

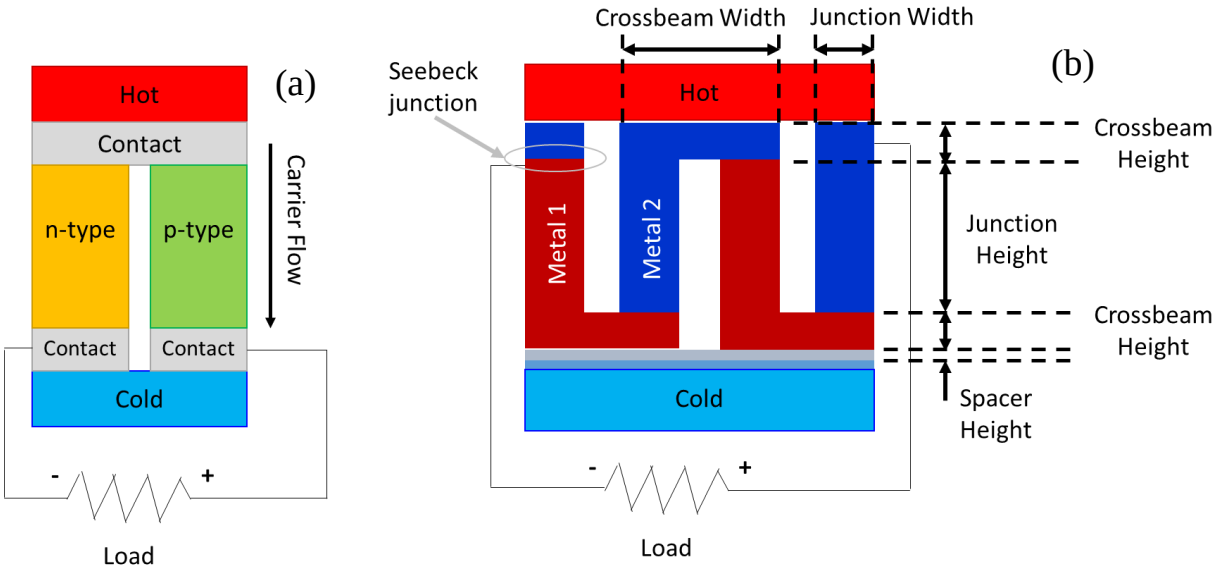

Figure 1. Comparison of conventional semiconductor-based thermoelectric concept (a) to the new metallic junction thermoelectric concept (b). The former relies on thermal migration of electrical carriers from the hot to the cold end to generate electrical potential, whereas the new concept uses the Seebeck effect at the junctions between the dissimilar metals. The higher electron concentration and carrier mobility inherent in metals enables higher power conversion efficiency. Relevant dimensions to be tested in the simulation are shown in (b).

Increased efficiency can be achieved with a different approach. Semiconductors are inherently limited in conductivity by the amount of dopant. Metals have a high thermal and electrical conductivity, and a large number of carriers compared to semiconductors. This combination is unacceptable for the device shown in Fig. 1a; carriers will recombine rather than conduct current through a load. Therefore, the design in Fig. 1b is proposed instead. This setup produces a net Seebeck effect voltage at each junction between metal 1 and metal 2 and drives a current through a load. No elaborate combination of material properties is necessary, only a pairing of metals that produces a high Seebeck voltage.

Many combinations of metals are possible, but the highest voltage, about 60μV/K, comes from Chromel-Constantan. Depending on the number of junctions, the output power is expected to be much higher than that from a current RTG in Fig. 1a. Several variables affect the efficiency. Metal post height increases the temperature gradient between junctions, and thus power output, but also increases thermal resistance, decreasing power output. Thicker crossbeams allow for easier current flow (more power), but increase thermal resistance (less power). Increasing junction density means more devices to generate power (more power), but the reduced device size lowers electrical and thermal conductivity (less power). More layers of metallic junctions increases the number of devices (more power), but also increases thermal resistance and flattens the temperature gradient (less power at each device). To balance these factors, a finite element model (FEM) of the design in Fig. 1b was constructed in Matlab.

2. SIMULATION SETUP

The metallic junction design was divided into a grid of rectangular areas, the finite elements, as shown in Fig. 2. Flux balance was tracked at each element, with the amount of heat entering and leaving from each of the four sides. Steady state heat flow was assumed at each edge for a time step small enough to approximate non-steady state heat flow. Also, a linear

temperature gradient was assumed as the initial temperature profile from the heat source T_{Hot} to the cold sink $T_{Ambient}$, greatly reducing the number of steps required for convergence. T_{Hot} and $T_{Ambient}$ were assumed constant through the simulation, easing the processing burden enough for computation on a standard desktop computer.

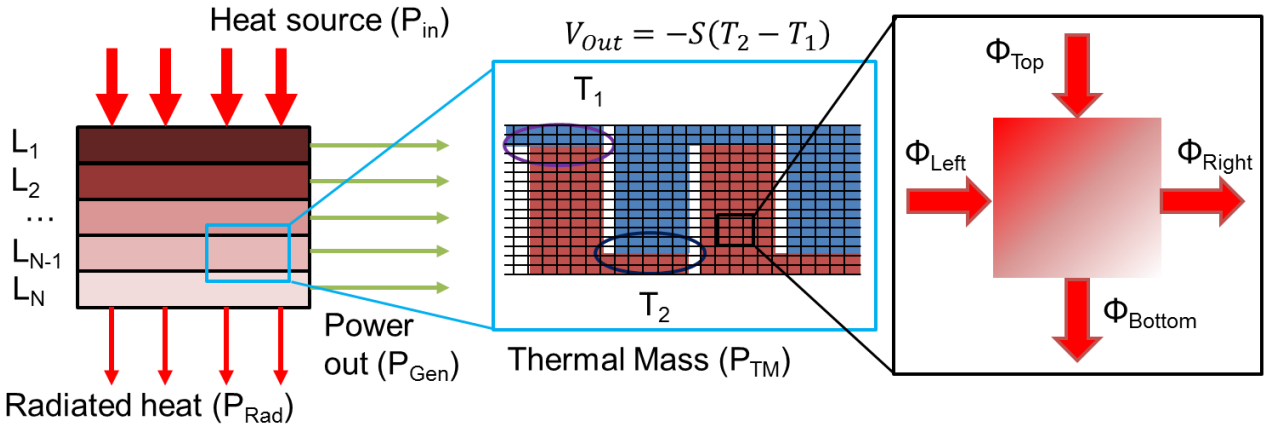

Figure 2. Setup of metallic junction FEM (left). Each layer consists of several junctions (middle), separated into several discrete elements (right). Each layer is represented as a single junction with looping boundary conditions; the thermal flux off the right side appears on the left edge, and vice versa. Constant temperature boundary conditions exist on the top of the top-most layer, where T is fixed at T_{Hot}, and likewise T is fixed at $T_{Ambient}$ for the bottom of the lowest layer.

Any net heat gain was calculated into a temperature increase according to the heat capacity and volume of the element, and likewise temperature losses for net heat losses. Resulting heat flux was then calculated. As such, the simulation was iterative, run for at least 100,000 iterations of alternating heat flux and temperature change calculations until convergence of temperature was obtained.

For a given device size and structure, several grid densities were simulated to obtain convergence on calculated efficiency. Lateral grid spacing is defined as the number of elements within a layer of the metallic junction device, while the vertical grid is the number of elements in the direction transverse to each layer. For most runs in this work, individual devices were roughly 80µm wide x 70µm tall, and the grid density was 50x75 in the lateral x vertical directions, corresponding to about 0.6µm x 1µm for each element. More than this did not show improved accuracy in the results, while fewer did not speed up the simulation appreciably. A typical thermal profile of the metallic junction device after reaching equilibrium is shown in Fig. 3.

Efficiency was measured through tracking the amount of thermal energy change in each element after each time step. Heat went 1 of 3 places: into electrical power generation ($P_{Generated}$), stored ($P_{ThermalMass}$) or released from the individual elements, or emitted as waste heat ($P_{WasteHeat}$), that is all the thermal flux downward from the bottom-most edge; this would be heat loss to a heat sink in a real device. No heat loss to the sides is permitted, as these will be insulated in a real device. Efficiency (η) was calculated as:

$$\eta = \frac{P_{Generated}}{P_{Generated} + P_{ThermalMass} + P_{WasteHeat}} \quad (2)$$

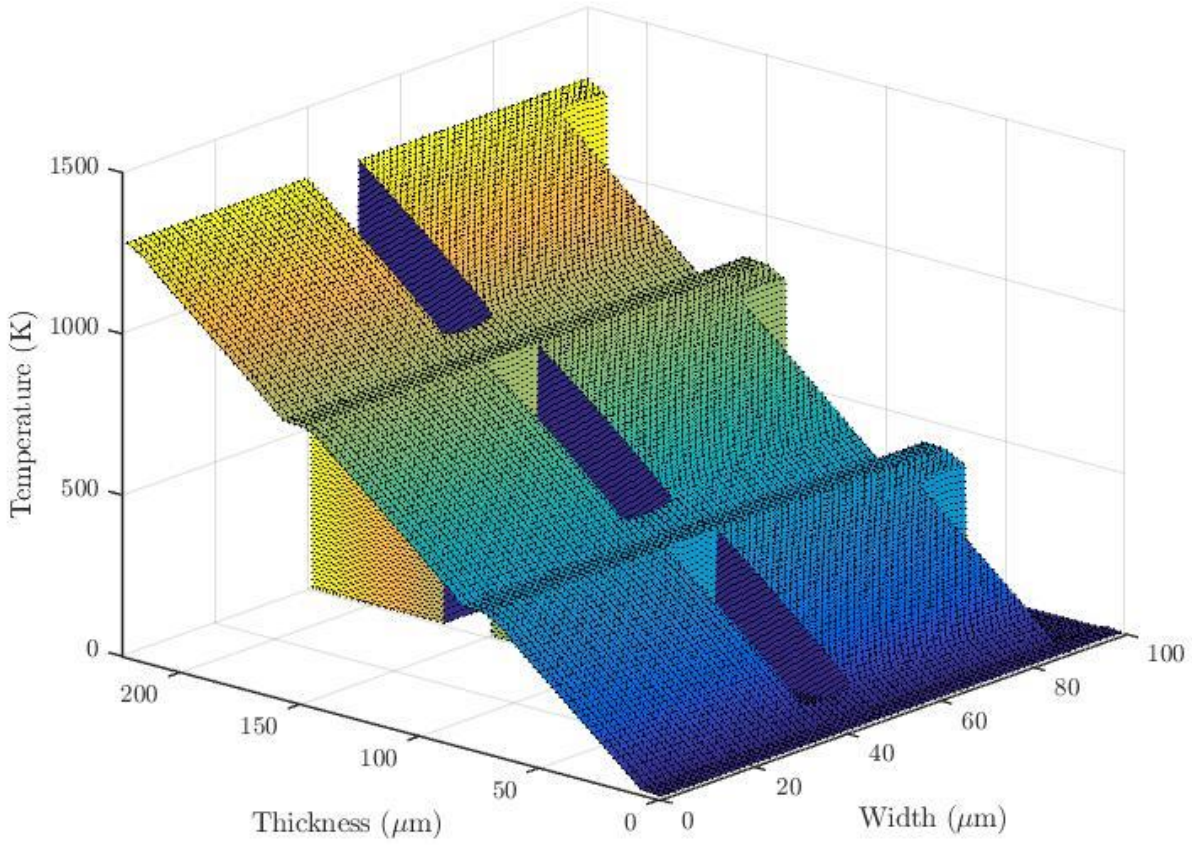

Figure 3. Typical thermal profile at steady state in a metallic junction device. T_{Hot} is 1273K, $T_{Ambient}$ is 3K.

3. RESULTS

Optimization started with a "standard" device configuration of 10 layers, 10^8 devices per layer, junction post height of 50μm, and crossbeam heights of 10μm. Starting with these wired in series, the efficiency as a function of $T_{Ambient}$ was calculated for a constant T_{Hot} = 1273K and is plotted in Fig. 4. According to these results, the efficiency follows a linear trend, consistent with the linear temperature gradients that form in the metallic portions of the junctions. The space layers have a flatter temperature profile, consistent with Si having a much higher thermal conductivity and heat capacity than the constituent metals.

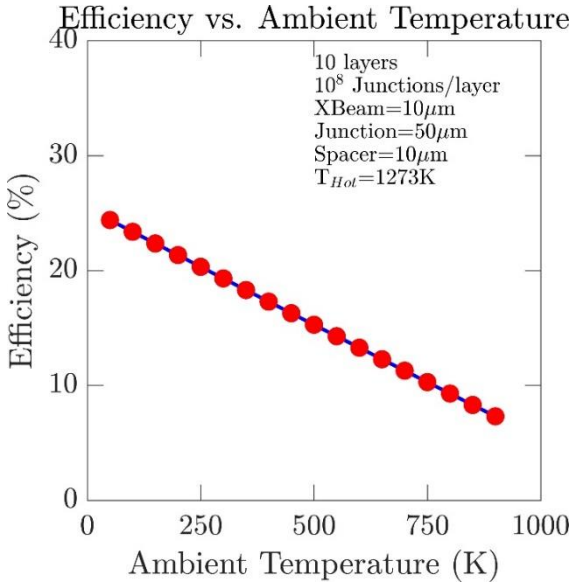

Figure 4. Efficiency as a function of $T_{Ambient}$.

Efficiency reaches a maximum of about 24% for these particular junction dimensions. Optimization of these dimensions began with the crossbeam height, plotted in Fig. 5. Efficiency increased from the starting height of 10µm, then reached a maximum of 38% at a height of 40µm, before dropping again with increasing crossbeam height. This is due to the competing factors listed above, namely, the larger height increases the amount of room for electron travel, decreasing electrical resistance, but also increasing the height for heat to pass through, increasing thermal resistance and thus restricting heat flow. The optimal balance for these two quantities is around 40µm, for a junction post height of 50µm and a spacer height of 10µm. Changing these dimensions may affect the optimal crossbeam height, requiring re-optimization.

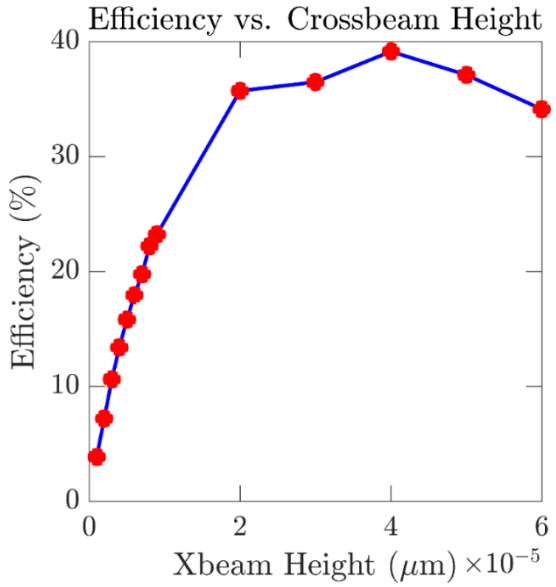

Figure 5. Efficiency as a function of crossbeam height, which peaks at about 38% at 40µm. Before this point, electrical resistance is higher than optimal, while after this point, thermal resistance is higher than optimal.

Efficiency vs T_{Hot} is given in Fig. 6. Efficiency of the metallic junction device scales linearly with heat source temperature vs. a 3K background temperature. Similar results (not shown) are achieved with a 293K background temperature, albeit with lower efficiencies. These results are not surprising, given the linear temperature gradient that exists within the device

layers; as T_{Hot} increases, the gradient becomes steeper, and thus the temperature difference between junctions causes an increased Seebeck effect.

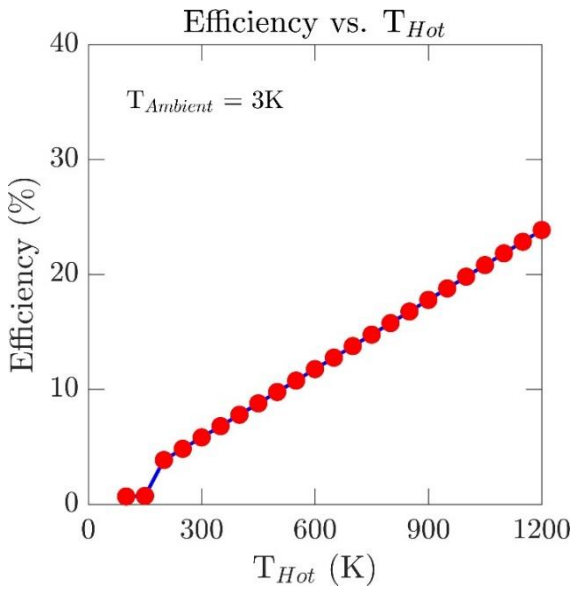

Figure 6. Efficiency vs. T_{Hot}. As with Fig. 4, a linear trend is observed, consistent with steady state temperature gradients.

Efficiency vs. number of layers is shown in Fig. 7. In constructing a metallic junction device, the number of layers increases the thermal and electrical resistance, but also harnesses more of the conducting heat. At about 8 layers, a consistent efficiency of ~25% is achieved, which does not increase with more layers.

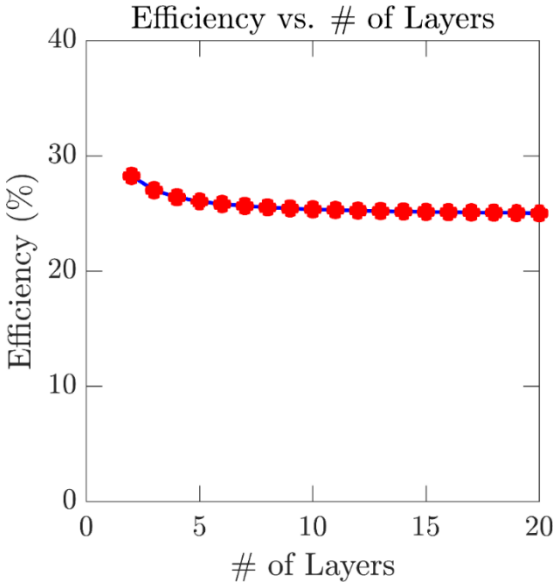

Figure 7. Efficiency vs. number of metallic junction layers. Efficiency gains and increased output voltage are balanced with increasing resistance as the number of layers increase, resulting in no real gain in efficiency past 8 layers.

The 2 and 3 layer devices appear to be more efficient, but in reality will likely not maintain a T_{Hot}-$T_{Ambient}$ temperature gradient. The lowest layer will heat up until the amount of radiation into ambient matches the heat flux into the lowest layer. That heating reduces the temperature gradient. Increasing the number of layers lowers the temperature gradient, spreading the temperature difference over an increasing height. This reduces the individual layer contributions to total

output power, resulting in the same amount of total device output, but reduced for the increase in electrical resistance. As the number of layers increases, the thermal mass increases, allowing more power to be drawn out as electricity before reaching the radiator below the bottom layer.

Efficiency as a function of the spacer layer height is shown Fig. 8. For these simulations, undoped silicon was proposed as the spacer material; any thermally conductive and electrically insulative material (i.e., diamond) would work well here. Not surprisingly, Fig. 8 shows a decrease in efficiency as the height increases, owing to increased thermal resistance and the higher heat capacity of Si. These properties siphon energy away from the metallic junctions, reducing the gradient between them. This effect is rather small, not changing the efficiency much for any height below 10μm. Above 10μm, the impact is greater. For a practical device, parasitic capacitance and thermal strain in the spacer might also need to be considered.

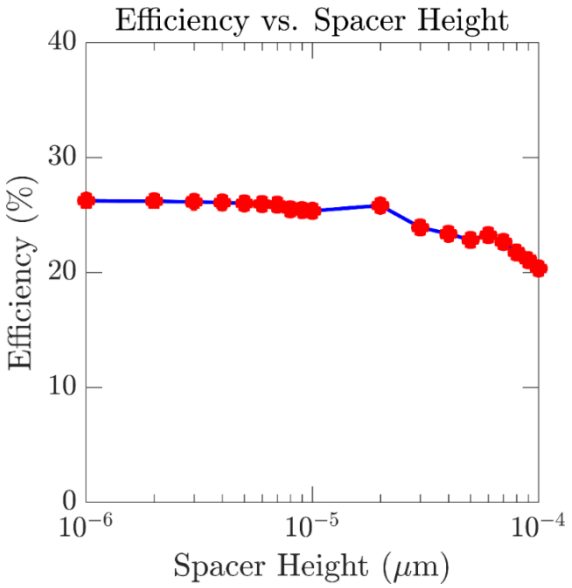

Figure 8. Efficiency vs. electrically insulating spacer height. Below 10μm, little is gained from decreasing the insulating layer height; capacitance effects become much larger, and thus a drop in efficiency is expected at very small (<1μm) heights.

4. DISCUSSION AND APPLICATIONS

Some efforts have been made to adapt conventional thermoelectric devices to human skin to harness power for low-power sensors and implants. These efforts produced at most 1 mW for large, bulky devices that were uncomfortable to wear and inconsistent in output due to changing ambient temperatures and clothing. The use of metallic junctions offers new possibilities.[37–44]

For wearable energy conversion fabric to be successful, the device needs to be flexible, yet sturdy. If the spacer layers between the metallic junction layers are sectioned to leave a gap between the junctions, flexibility is quite possible, and with only 10s of layers at most, the total height should not exceed 1mm. Encased in a thin, flexible shell for protection and durability, the packaged device could be adapted for any shape and area. Figure 5 shows 38% efficiency is possible, a 5 fold increase over current technology, making 5mW of power possible, enough to power medical sensors, implants, and low-power wireless devices.

Vehicle engines and other heat sources provide another application area. Most engine heat is wasted as exhaust, while some of the usable work output powers a radiator to keep the engine from overheating. Leveraging the high engine heat with the forced cooling gives a high T_{Hot} and a lower $T_{Ambient}$. Hence, efficiencies of 10-20% are quite possible, supplying electrical power for continuing combustion (in place of a battery) and to various onboard devices.

Deep space probes benefit the most, thanks to the high difference between T_{Hot} (1273K) and $T_{Ambient}$ (3K). Pu^{238} is the isotope of choice in RTG construction as it has a high decay heat of ~1273K and primarily emits easily-contained alpha

particles. However, stockpiles are tightly limited and difficult to produce as production requires a particle accelerator. Reducing the required amount to only about 1/5 the usual amount alleviates this tremendously. Missions that require more power would be possible, and this increases the feasibility of long-term manned missions into the solar system.[45–50]

5. CONCLUSION

An alternative to the traditional semiconductor-based thermoelectric device was proposed. Using bimetallic junctions in place of n- and p-doped semiconductors, much higher carrier mobilities and concentrations are possible, increasing potential power output. This also circumvents the figure of merit problem that requires high electrical conductivity and low thermal conductivity to coexist in the same material. Two-dimensional FEM simulations were performed to predict an optimized device structure, balancing competing factors to achieve over 35% conversion efficiency, vs 7% for traditional thermoelectric devices. While experimental verification remains for future microfabrication work, energy harvesting to power low-power devices from human body heat and mechanical engines and the impacts on deep space power production were discussed.

REFERENCES

[1] Narducci, D., "Do we really need high thermoelectric figures of merit? A critical appraisal to the power conversion efficiency of thermoelectric materials," Appl. Phys. Lett. **99**(10), 17–20 (2011).

[2] Stordeur, M.., Stark, I., "Low power thermoelectric generator - self-sufficient energy supply for micro systems," 16th Int. Conf. Thermoelectr., 575–577 (1997).

[3] National Aeronautics and Space Administration., "Radioisotope power systems: radioisotope thermoelectric generator (RTG)," 2013, <https://solarsystem.nasa.gov/rps/rtg.cfm> (6 January 2017).

[4] Koelle, D.., Janovsky, R., "Development and transportation costs of space launch systems," Proc. DGLR/CEAS Eur. Air Sp. Conf. (2007).

[5] Swanson, R. M., "A proposed thermophotovoltaic solar energy conversion system," Proc. IEEE **67**(3), 446–447 (1979).

[6] Schock, A., Mukunda, M., Or, C., Kumar, V.., Summers, G., "Design, analysis, and optimization of a radioisotope thermophotovoltaic (RTPV) generator, and its applicability to an illustrative space mission," Acta Astronaut. **37**(C), 21–57 (1995).

[7] Ferrari, C., Melino, F., Pinelli, M., Spina, P. R.., Venturini, M., "Overview and status of thermophotovoltaic systems," Energy Procedia **45**, 160–169 (2014).

[8] Bermel, P., Ghebrebrhan, M., Chan, W., Yeng, Y. X., Araghchini, M., Hamam, R., Marton, C. H., Jensen, K. F., Soljačić, M., et al., "Design and global optimization of high-efficiency thermophotovoltaic systems.," Opt. Express **18 Suppl 3**(103), A314–A334 (2010).

[9] Nelson, R. E., "A brief history of thermophotovoltaic," Semicond. Sci. Technol. **18**, S141–S143 (2003).

[10] Crowley, C. J., Elkouh, N. A., Murray, S.., Chubb, D. L., "Thermophotovoltaic converter performance for radioisotope power systems," AIP Conf. Proc. **746**, 601–614 (2005).

[11] Coutts, T. J., "Overview of thermophotovoltaic generation of electricity," Sol. Energy Mater. Sol. Cells **66**(1–4), 443–452 (2001).

[12] Murray, C. S., Crowley, C. J., Murray, S., Elkouh, N. A., Hill, R. W.., Chubb, D. E., "Thermophotovoltaic converter design for radioisotope power systems," AIP Conf. Proc. Thermophotovoltaic Gener. Electr. 6th Conf., 123–132 (2004).

[13] Molesky, S.., Jacob, Z., "Ideal near-field thermophotovoltaic cells," Phys. Rev. B **91**(20), 1–7 (2015).

[14] Sulima, O. V.., Bett, A. W., "Fabrication and simulation of GaSb thermophotovoltaic cells," Sol. Energy Mater. Sol. Cells **66**(1–4), 533–540 (2001).

[15] Coutts, T. J., "Review of progress in thermophotovoltaic generation of electricity," Renew. Sustain. energy Rev.

3(2), 77–184 (1999).

[16] Shakouri, A., “Thermoelectric , thermionic and thermophotovoltaic energy conversion J Q (r) q Report Documentation Page” (2005).

[17] Rosaire, C. G., Heinemann, M. J., MacLachlan, C. S.., Howe, S. D., “Radioisotope thermophotovoltaic batteries for universal low power systems,” Nucl. Emerg. Technol. Space, NETS 2013, 419–427 (2013).

[18] Cheetham, K. J., Carrington, P. J., Cook, N. B.., Krier, A., “Low bandgap GaInAsSbP pentanary thermophotovoltaic diodes,” Sol. Energy Mater. Sol. Cells **95**(2), 534–537, Elsevier (2011).

[19] Nagpal, P., Han, S. E., Stein, A.., Norris, D. J., “Efficient low-temperature thermophotovoltaic emitters from metallic photonic crystals,” Nano Lett. **8**(10), 3238–3243 (2008).

[20] Durisch, W.., Bitnar, B., “Novel thin film thermophotovoltaic system,” Sol. Energy Mater. Sol. Cells **94**(6), 960–965, Elsevier (2010).

[21] Schock, A., Or, C.., Kumar, V., “Design and integration of small RTPV generators with new millennium spacecraft for outer solar system,” Acta Astronaut. **41**(12), 801–816 (1997).

[22] Gerstenmaier, Y. C.., Wachutka, G., “Efficiency of thermionic and thermoelectric converters,” AIP Conf. Proc. **890**, 37–46 (2007).

[23] Oman, H., “Deep space travel energy sources,” IEEE Aerosp. Electron. Syst. Mag. **18**(2), 28 (2003).

[24] Humphrey, T. E., O’Dwyer, M. F.., Linke, H., “Power optimization in thermionic devices,” J. Phys. D. Appl. Phys. **38**(12), 2051–2054 (2005).

[25] Trucchi, D. M., Bellucci, A., Cappelli, E., Calvani, P., Orlando, S., Sciti, D., Yogev, R.., Kribus, A., “Thermionic Emission : A Different Path to Solar Thermal Electricity,” SolarPaces Conf. (2012).

[26] Schwede, J. W., Bargatin, I., Riley, D. C., Hardin, B. E., Rosenthal, S. J., Sun, Y., Schmitt, F., Pianetta, P., Howe, R. T., et al., “Photon-enhanced thermionic emission for solar concentrator systems,” Nat. Mater. **9**(9), 762–767, Nature Publishing Group (2010).

[27] Adams, S. F., “Solar thermionic space power technology testing: A historical perspective,” AIP Conf. Proc. **813**, 590–597 (2006).

[28] Ha, C. T., Fernandez, R., Cornford, S. L.., Feather, M. S., “Advanced stirling radioisotope generator: Design processes, reliability analyses impacts, and extended operation tests,” AIP Conf. Proc. **969**, 458–465 (2008).

[29] Chan, J., Wood, J. G.., Schreiber, J. G., “Development of advanced Stirling Radioisotope Generator for space exploration,” AIP Conf. Proc. **880**(May), 615–623 (2007).

[30] Wong, W. A., Wood, J. G.., Wilson, K., “Advanced Stirling convertor (ASC) - from technology development to future flight product,” 1–26 (2008).

[31] Cockfield, R. D.., Chan, T. S., “Stirling radioisotope generator for mars surface and deep space missions,” 2002 37th Intersoc. Energy Convers. Eng. Conf., 134–139 (2002).

[32] Shaltens, R. K.., Wong, W. A., “Advanced Stirling technology development at NASA Glenn Research Center,” NASA Sci. Technol. Conf.(September) (2007).

[33] Oriti, S. M., “Advanced Stirling Radioisotope Generator Engineering Unit 2 (ASRG EU2) final assembly” (2015).

[34] Mason, L. S., Schifer, N. A.., Glenn, N., “Modular stirling radioisotope generator,” 13th Int. Energy Convers. Eng. Conf., 3809 (2015).

[35] Chan, T. S., “System-level testing of the advanced Stirling radioisotope generator engineering hardware,” 12th Int. Energy Convers. Eng. Conf. (2014).

[36] Chan, J., Hill, D., White, J.., Elisii, R., “Advanced stirling radioisotope generator emergency heat dump test for nuclear safety consideration,” 9th Annu. Int. Energy Convers. Eng. Conf. IECEC 2011 (2011).

[37] Leonov, V.., Vullers, R. J. M., “Wearable thermoelectric generators for body-powered devices,” J. Electron. Mater. **38**(7), 1491–1498 (2009).

[38] Leonov, V., Van Hoof, C.., Vullers, R. J. M., “Thermoelectric and hybrid generators in wearable devices and clothes,” Proc. - 2009 6th Int. Work. Wearable Implant. Body Sens. Networks, BSN 2009, 195–200 (2009).

[39] Wang, Z., Leonov, V., Fiorini, P.., Van Hoof, C., “Realization of a wearable miniaturized thermoelectric generator for human body applications,” Sensors Actuators, A Phys. **156**(1), 95–102 (2009).

[40] Leonov, V., “Thermoelectric energy harvesting of human body heat for wearable sensors,” IEEE Sens. J. **13**(6), 2284–2291 (2013).

[41] Kim, M. K., Kim, M. S., Jo, S. E., Kim, H. L., Lee, S. M.., Kim, Y. J., “Wearable thermoelectric generator for human clothing applications,” 2013 Transducers Eurosensors XXVII 17th Int. Conf. Solid-State Sensors, Actuators Microsystems(June), 1376–1379 (2013).

[42] He, W., Zhang, G., Zhang, X., Ji, J., Li, G.., Zhao, X., “Recent development and application of thermoelectric generator and cooler,” Appl. Energy **143**, 1–25 (2015).

[43] Bahk, J.-H., Fang, H., Yazawa, K.., Shakouri, A., “Flexible thermoelectric materials and device optimization for wearable energy harvesting,” J. Mater. Chem. C **3**, 10362–10374 (2015).

[44] Sebald, G., Guyomar, D.., Agbossou, A., “On thermoelectric and pyroelectric energy harvesting,” Smart Mater. Struct. **18**(12), 125006 (2009).

[45] Miotla, D., “Assessment of plutonium-238 production alternatives,” 2008, <http://energy.gov/sites/prod/files/NEGTN0NEAC_PU-238_042108.pdf> (30 January 2016).

[46] National Aeronautics and Space Administration., “What is plutonium-238 ?,” <https://solarsystem.nasa.gov/rps/docs/APP RPS Pu-238 FS 12-10-12.pdf> (25 January 2016).

[47] Howe, S. D., Crawford, D., Navarro, J.., Ring, T., “Economical production of Pu-238,” Nucl. Emerg. Technol. Sp. (NETS 2013) **238**, 1–12 (2013).

[48] Wall, M., “Full-Scale Production of Plutonium Spacecraft Fuel Still Years Away,” Space.com, 2016, <http://www.space.com/32890-nuclear-fuel-spacecraft-production-plutonium-238.html> (15 December 2016).

[49] Griggs, M. B., “Plutonium-238 is produced in America for the first time in almost 30 Years,” Pop. Sci., 2015, <http://www.popsci.com/plutonium-238-is-produced-in-america-for-first-time-in-30-years> (15 December 2016).

[50] Szondy, D., “US restarts production of plutonium-238 to power space missions,” New Atlas, 2015, <http://newatlas.com/ornl-plutonium-238-production-space/41041/> (15 December 2016).